forests

MDPI

Article

Sub-Canopy Topography Retrieval Using FVC-Integrated TanDEM-X Dual-Baseline InSAR

Zhimin Feng [1,2], Huiqiang Wang [1,2], Ruiping Li [1,2,*], Xiangwei Meng [3,4], Liying Zhou [5] and Xiaoming Ma [5]

[1] College of Water Conservancy and Civil Engineering, Inner Mongolia Agricultural University, Hohhot 010018, China; fengzm@emails.imau.edu.cn (Z.F.); huiqiangwang@imau.edu.cn (H.W.)
[2] State Key Laboratory of Water Engineering Ecology and Environment in Arid Area, Inner Mongolia Agricultural University, Hohhot 010018, China
[3] Xilinhot Meteorological Bureau, Xilinhot 026000, China; 4250108011@stu.cuit.edu.cn
[4] School of Atmospheric Sciences, Chengdu University of Information Technology, Chengdu 610225, China
[5] Water Resources Research Institute of Inner Mongolia Autonomous Region, Hohhot 010051, China; zhouliying0817@163.com (L.Z.); maxiaoming@emails.imau.edu.cn (X.M.)
* Correspondence: nmglrp@imau.edu.cn

Abstract

Conventional Interferometric Synthetic Aperture Radar (InSAR)-based sub-canopy topography retrieval models often suffer from insufficient characterization of scattering mechanisms, strong nonlinearity, and poor parameter convergence. To address these issues, this study proposes an improved Interferometric Water Cloud Model (IWCM) that integrates Fractional Vegetation Cover (FVC) to retrieve sub-canopy topography. The proposed method accounts for both volume and ground scattering and introduces FVC as a constraint to improve the model's physical realism. In addition, this study utilizes InSAR observations derived from TanDEM-X dual-baseline data, which enhance the information content of the measurements by providing multiple independent interferometric observations. A two-step nonlinear least squares optimization strategy is further employed to enhance the convergence of model parameter estimation. The proposed method was validated in the forested region of Genhe City, Inner Mongolia. Airborne LiDAR-derived surface elevation data were used for assessment. The results indicate that, compared with the original InSAR-derived Digital Elevation Model (DEM), the accuracy of the retrieved sub-canopy topography improves by 39.04%. Furthermore, compared with the previously proposed Normalized Difference Vegetation Index (NDVI)-based method, under their respective optimal initial extinction coefficient conditions (μ_0), an additional accuracy improvement of 11.69% is achieved. These results demonstrate that the proposed method effectively reduces the influence of the forest canopy on interferometric phase observations and improves the capability of sub-canopy topography reconstruction in complex forest environments. The method also provides a new approach for dual-baseline and multi-baseline InSAR-based sub-canopy topography retrieval.

Keywords: sub-canopy topography; dual-baseline InSAR; Interferometric Water Cloud Model (IWCM); Fractional Vegetation Cover (FVC)

Check for updates

Academic Editor: Aleksandar Dj Valjarević

Received: 1 April 2026
Revised: 4 May 2026
Accepted: 8 May 2026
Published: 9 May 2026

Copyright: © 2026 by the authors. Licensee MDPI, Basel, Switzerland. This article is an open access article distributed under the terms and conditions of the Creative Commons Attribution (CC BY) license.

1. Introduction

The Digital Elevation Model (DEM) is a fundamental geospatial dataset that supports a wide range of applications, including natural disaster prevention and mitigation, infrastructure development, economic growth, and national security [1–3]. The spaceborne

Interferometric Synthetic Aperture Radar (InSAR) system, as an advanced active microwave remote sensing technology, has demonstrated unique advantages in topographic mapping owing to its stable Earth observation capability [4]. With its day-and-night and all-weather observation capability, InSAR has become one of the most important techniques for acquiring surface elevation information at regional and even global scales due to its high measurement accuracy and wide spatial coverage [5–7]. However, in forest-covered areas, the interaction between forest targets and the SAR signal often means that the elevation measured by InSAR corresponds to the scattering phase center located between the forest canopy and the ground surface. This leads to an unknown elevation bias in terrain measurements, particularly in the retrieval of sub-canopy topography [8]. Therefore, InSAR-based high-precision sub-canopy topography retrieval requires accurate mitigation of the elevation bias, which is referred to as the scattering phase center height (SPCH).

The estimation and calibration of the SPCH should take into account SAR backscattering processes or the SAR scattering mechanism in forest-covered areas. The existing research can be divided into two categories. The first category considers only the volume scattering process from the forest canopy and typically assumes that ground scattering can be neglected. Representative approaches include coherence-based empirical and semi-empirical models, regression models, and the SINC model derived from the simplification of the Random Volume over Ground (RVoG) model [9–11]. These methods model complex scattering mechanisms by establishing relationships between coherence and forest parameters. Specifically, they focus on volume scattering from the forest canopy while ignoring or implicitly treating ground scattering. This simplification reduces the model's dimensionality and the number of unknown parameters. As a result, the dependence on input data and prior information is reduced, thereby alleviating the ill-posedness of the inversion process. At the same time, the computational complexity is significantly decreased, improving both the efficiency and stability of the algorithm. However, because the ground scattering component is ignored, the description of the forest scattering process remains incomplete, which limits their applicability in complex forest environments (such as boreal forest areas with heterogeneous densities) [12–14]. The second category considers both ground scattering and volume scattering, as in the RVoG model and IWCM [15–17]. These methods provide a more comprehensive representation of forest scattering mechanisms. However, due to the increased complexity of the inversion model and the larger number of unknown parameters, model inversion often requires additional constraints, such as polarimetric interferometric data, external auxiliary data, multi-baseline InSAR data, etc. [18–21].

In boreal forest environments, forest density typically exhibits significant spatial heterogeneity in the horizontal direction [22]. This variation directly affects the relative contributions of ground and volume scattering. Therefore, an appropriate representation of forest density is essential for accurately characterizing the scattering process and improving model performance. In this context, the Interferometric Water Cloud Model (IWCM) provides a more physically meaningful framework for SAR scattering processes by describing the forest density. The model represents the forest volume as a random medium with gaps above the ground surface and accounts for the combined effects of ground scattering and volume scattering, making it suitable for forests with heterogeneous density distributions [23–25]. In previous work, the Normalized Difference Vegetation Index (NDVI) was used to characterize vegetation conditions [17].

In this study, Fractional Vegetation Cover (FVC) is introduced as an indicator of forest density. Compared with the NDVI, FVC more directly reflects the horizontal coverage of vegetation and has a clearer physical meaning. In addition, FVC is used to constrain the relative contributions of ground scattering and volume scattering, thereby improving the stability and physical consistency of the inversion model. In model inversion, strong nonlin-

earity and parameter coupling make it difficult to obtain stable solutions using conventional direct inversion methods. Nonlinear relationships may lead to multiple local minima, while parameter coupling introduces non-uniqueness, making the results highly sensitive to initial values and noise [15–17]. To address this issue, a two-step iterative optimization strategy is adopted. First, initial parameter estimates are obtained under predefined constraints. Then, in the second stage, the solution is further optimized using these initial values, allowing it to gradually converge toward the true solution. The study area is located in the forest region of Genhe City in northeastern Inner Mongolia. The datasets include TanDEM-X dual-baseline InSAR observations, ICESat-2 surface elevation data, and airborne LiDAR-derived elevation data, which are used for model validation and comparative analysis.

Compared with existing studies, the main contributions of this work are as follows: (1) An FVC-constrained interferometric scattering model (IWCM) is proposed. It improves the physical consistency of vegetation scattering modeling. It also better represents forest structural heterogeneity. (2) Dual-baseline InSAR data are used to increase the number of independent observations. This improves the robustness of parameter inversion. (3) A two-step nonlinear optimization strategy is adopted. This reduces the effects of strong nonlinearity and parameter coupling. (4) The relationships among forest density, terrain slope, and the model parameter μ_0 are systematically analyzed. This provides new insights into the retrieval of sub-canopy topography in complex forest environments.

2. Study Area and Data Description

2.1. Overview of the Study Area

The study area is located in the northern section of the Greater Khingan Mountains in northeastern Inner Mongolia Autonomous Region, China, and is administratively under the jurisdiction of Genhe City. The geographic extent of the study area ranges from 120°28′–122°39′ E and 50°52′–51°00′ N (Figure 1a). According to climatic classification, the region belongs to a cold-temperate humid climate zone, characterized by pronounced seasonal variations. Winters are long and extremely cold, whereas summers are relatively short and generally cool. The region receives an average annual precipitation of approximately 450 mm, and the frost-free period typically lasts 80–90 days. Under such climatic conditions, forest vegetation in the study area is dominated by tree species adapted to low-temperature environments and capable of maintaining stable growth.

The Genhe forest region is located on the western slope of the northern Greater Khingan Mountains. The terrain is primarily characterized by undulating mountains, with considerable topographic variation. Surface slopes within the region mainly range from 0° to 30°, providing favorable terrain conditions for the extensive distribution of forest vegetation. Forest resources in the region are relatively well preserved, with a forest coverage rate of approximately 91.7%, making it one of the regions with the highest forest coverage in northern China. In terms of forest composition, *Larix gmelinii* (*Dahurian larch*) dominates the region, accounting for more than 70% of the total forest area. In addition, coniferous species such as *Pinus sylvestris* var. *mongolica* and *Picea* are distributed in the region, alongside broadleaf species including *Betula platyphylla* and *Populus davidiana*, forming a mixed forest community.

Under the combined influence of terrain and elevation gradients, forest types in the study area exhibit distinct vertical zonation in their spatial distribution. Generally, areas with elevations exceeding 1000 m are mainly dominated by pure stands of *Larix gmelinii*, whereas forests at lower elevations are more commonly composed of mixed coniferous and broadleaf species. This vegetation pattern reflects clear vertical structural differences and highlights the important role of elevation in controlling the spatial distribution of forest types in the region (information available online: https://www.genhe.gov.cn/About/ (accessed on 5 May 2026)).

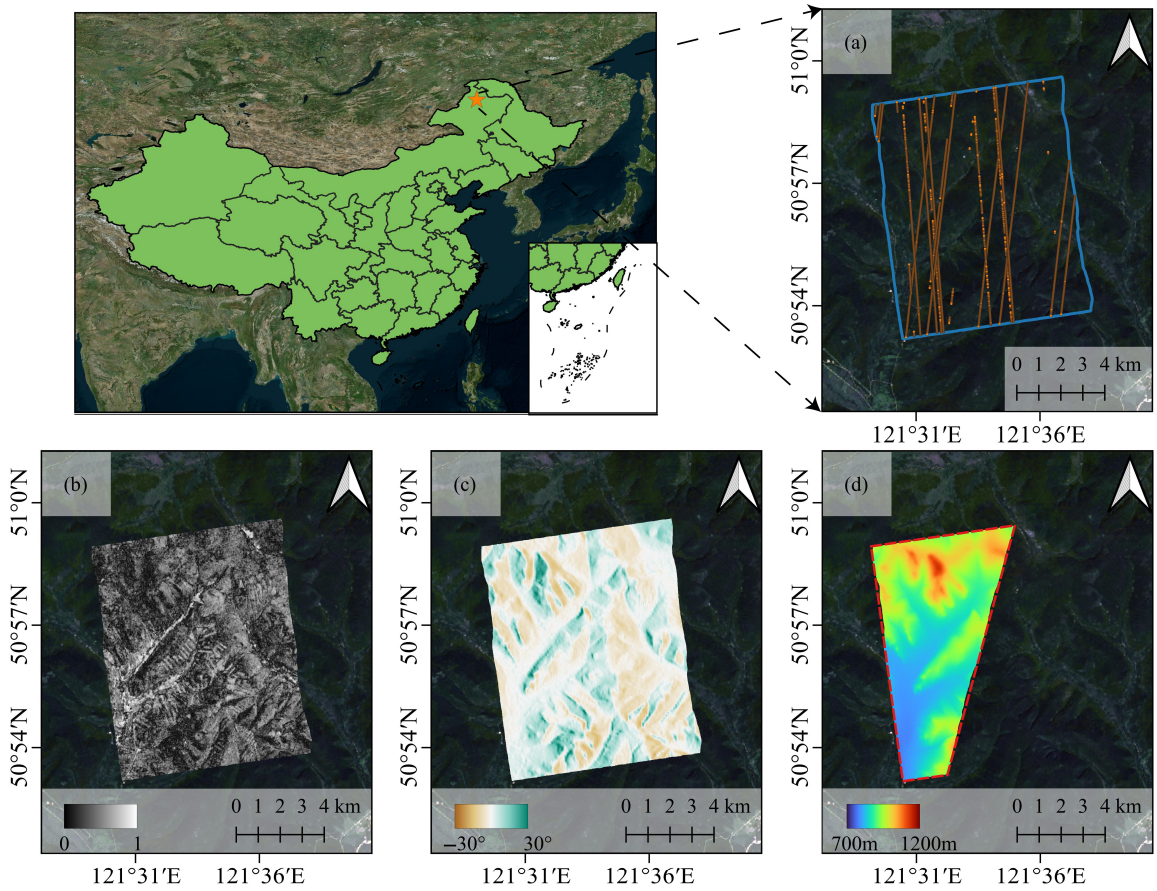


Figure 1. Overview of the Genhe study area: (**a**) extent of the study area (orange dots indicate ICESat-2 surface elevation points; blue solid box indicates the extent of the study area); (**b**) interferometric coherence map; (**c**) slope distribution of the study area; (**d**) LiDAR-derived surface elevation.

2.2. TanDEM-X Bistatic InSAR Data

TanDEM-X is an Earth observation mission launched by the German Aerospace Center (DLR). It consists of two nearly identical X-band satellites, TerraSAR-X and TanDEM-X, operating in close formation. By employing bistatic InSAR observations, the mission effectively reduces temporal decorrelation. It partially mitigates atmospheric effects, enabling the generation of high-precision DEM data with near-global coverage [26–28]. In this study, TanDEM-X dual-baseline InSAR data covering the study area were acquired (Figure 1b). The detailed interferometric parameters are listed in Table 1.

Table 1. Geometric parameters of TanDEM-X CoSSC data.

InSAR Interferometric Data	Interferometric Pair 1	Interferometric Pair 2
Acquisition date	3 July 2016	14 July 2016
Effective baseline (m)	41.49	41.48
Incidence angle (°)	−312.11	−319.50
Polarization mode	HH	HH

2.3. FVC Product

FVC was estimated using optical imagery acquired from the Landsat 8 satellite provided by the United States Geological Survey (USGS), Reston, VA, USA [29]. During spring, vegetation enters the regreening and leaf expansion stages, while in autumn it undergoes senescence. These seasonal transitions often lead to unstable FVC values, which may not accurately reflect vegetation growth conditions. Although coniferous forests maintain canopy cover during colder periods, low temperatures suppress chlorophyll activity, resulting

in lower FVC values and reduced sensitivity compared with those observed in summer. Consequently, FVC data from other seasons are less suitable for vegetation monitoring. Therefore, a Landsat 8 image acquired on 1 August 2016, representing summer conditions, was selected for FVC estimation.

Based on the original Landsat 8 imagery, several preprocessing steps were performed, including cloud removal, spatial resampling, and clipping to the study area, to generate optical remote sensing data with a spatial resolution consistent with that of the InSAR data. The FVC values were subsequently calculated from the preprocessed imagery.

2.4. ICESat-2 Laser Altimetry Data

The ICESat-2 data used in this study were obtained from the Ice, Cloud, and Land Elevation Satellite-2 mission launched by the National Aeronautics and Space Administration (NASA). Previous studies have demonstrated that the ATL08 product provides high accuracy and reliability for retrieving surface elevation information [30]. Therefore, the ATLAS data from the ICESat-2 mission were used as the reference data to validate the sub-canopy topography retrieval results.

To reduce potential errors caused by temporal differences among datasets, ICE-Sat-2 surface elevation data acquired between May and September from 2019 to 2023 were selected for validation. A total of 4943 valid sample points were obtained, and their spatial distribution is shown by the yellow points in Figure 1a. This time period was chosen because the study area is typically snow-free during these months, while vegetation conditions remain relatively stable, facilitating the acquisition of reliable ground elevation measurements.

2.5. Airborne LiDAR Data

To further evaluate the accuracy of the sub-canopy topography retrieval results, airborne LiDAR-derived surface elevation data acquired over the study area were used as high-precision reference data. In 2024, airborne LiDAR data with a spatial resolution of 1 m $\times$ 1 m were collected over the Genhe study area. To ensure consistency with the InSAR data in terms of spatial resolution, the LiDAR-derived terrain data were resampled to 10 m $\times$ 10 m. The region overlapping with the InSAR coverage was then selected for comparison, as indicated by the black dashed box in Figure 1d. The LiDAR dataset has vertical accuracy better than 1 m, enabling it to reliably represent the true terrain conditions of the study area.

To improve the reliability and comprehensiveness of the validation, both ICESat-2 and airborne LiDAR datasets were used to assess accuracy. ICESat-2 data provide wide spatial coverage and a large number of sampling points, making them suitable for evaluating overall accuracy at the study area scale. In comparison, airborne LiDAR data offer higher spatial resolution and measurement accuracy, which makes them well-suited as high-precision reference data for local-scale validation. By combining the discrete ICESat-2 elevation samples with high-resolution LiDAR-derived terrain data, the accuracy of sub-canopy topography retrieval can be assessed across multiple spatial scales, thereby improving the robustness of the validation.

3. InSAR-Based Sub-Canopy Topography Retrieval Method

3.1. Improved IWCM with FVC Constraint

The IWCM is formulated within a theoretical framework based on several observables, including the backscattering coefficient, interferometric coherence, and phase height. The backscattering term in the model stems from the basic concept of the water cloud model, which assumes that scattering within a forest pixel comprises two components: volume

scattering from the vegetation layer and ground scattering from the surface. By introducing the forest canopy fill factor, which represents the proportion of forest coverage within a resolution cell, the total backscattering coefficient of a forested area (σ^0_{for}) can be expressed as follows [22]:

$$\sigma^0_{for} = \eta\left[\sigma^0_{gr}e^{-\alpha h} + \sigma^0_{veg}\left(1 - e^{-\alpha h}\right)\right] + (1-\eta)\sigma^0_{gr} \quad (1)$$

where η is the forest canopy fill factor, σ^0_{gr} represents the pure ground scattering contribution, and σ^0_{veg} denotes the pure volume scattering contribution. h is the forest height, and α is the attenuation coefficient. To describe the relative contributions of ground scattering and volume scattering, μ is introduced as the ground-to-volume amplitude ratio [31]

$$\mu = \mu_0 \frac{1 - \eta\left(1 - e^{-\alpha h}\right)}{\eta\left(1 - e^{-\alpha h}\right)} \quad (2)$$

where the pure ground-to-volume amplitude ratio μ_0 is defined as $\mu_0 = \sigma^0_{gr}/\sigma^0_{veg}$. Under interferometric observation conditions, the total scattering within a pixel can be regarded as the superposition of ground scattering and volume scattering. Therefore, the InSAR coherence can be expressed as a weighted combination of these two scattering contributions:

$$\tilde{\gamma} = \gamma_{sys}\left(\mu_{veg}\tilde{\gamma}_{vol} + \mu_{gr}\right) \quad (3)$$

where γ_{sys} represents the zero-height coherence, μ_{veg} denotes the weight of the volume scattering contribution, and μ_{gr} represents the weight of the ground scattering contribution. According to the energy conservation relationship of scattering, the weights can be expressed as

$$\begin{cases} \mu_{veg} = \frac{1}{1+\mu} \\ \mu_{gr} = \frac{\mu}{1+\mu} \end{cases} \quad (4)$$

where $\tilde{\gamma}_{vol}$ denotes the volume scattering coherence of the forest canopy. Physically, it represents the decorrelation effect caused by the random vertical distribution of scatterers within the vegetation layer. This coherence term can be calculated by integrating the scattering intensity distribution along the vertical direction, expressed as follows [31]:

$$\tilde{\gamma}_{vol} = \frac{\int_{-\infty}^{+\infty}\sigma(z)e^{jk_z z}dz}{\int_{-\infty}^{+\infty}\sigma(z)dz} = \frac{\alpha}{\alpha + jk_z}\frac{e^{jk_z h} - e^{-\alpha h}}{1 - e^{-\alpha h}} \quad (5)$$

where z represents the height within the vegetation volume scattering layer. k_z denotes the effective vertical wavenumber. The term $e^{-\alpha h}$ represents the two-way attenuation of vegetation, which characterizes the energy loss of the electromagnetic wave as it propagates through the vegetation scattering medium.

To enhance the model's capability to represent vegetation scattering characteristics, this study replaces the forest canopy fill factor in the conventional IWCM, which is difficult to obtain directly, with FVC. FVC is introduced as a constraint on the scattering weights, thereby leading to the formulation of an FVC-integrated IWCM, expressed as follows:

$$\tilde{\gamma} = \gamma_{sys}\left(\mu_{veg,FVC}\tilde{\gamma}_{vol} + \mu_{gr,FVC}\right) \quad (6)$$

3.2. Sub-Canopy Topography Retrieval Using TanDEM-X Dual-Baseline InSAR

The TanDEM-X bistatic satellite system enables the acquisition of high-precision interferometric phase information through synchronized interferometric observations, providing an important data source for terrain retrieval in forested areas. Compared with single-baseline InSAR, dual-baseline data provide additional observational dimensions

for the stability of model parameter estimation. In this study, the model parameters were estimated using dual-baseline InSAR coherence as the observations, with the pure ground-to-volume amplitude ratio set to $\mu_0 = 0.55$ [16]. The nonlinear least squares method (Equation (7)) was applied to estimate the forest height h and the attenuation coefficient α in the model. Because the nonlinear least squares algorithm is sensitive to initial parameter values, a penetration depth parameter was introduced as an additional constraint to improve solution robustness, following the approach proposed by Wang et al. [32].

$$(\alpha, h) = \arg\min_{\alpha,h} \sum_{i=1}^{n} \left\| \left| \tilde{\gamma}_{obs} \right|_i - \left| \tilde{\gamma}(\alpha, h) \right|_i \right\|^2 \tag{7}$$

In the least squares formulation, α and h are treated as the unknown parameters of the objective function, while n denotes the number of InSAR interferometric pairs. $\left|\tilde{\gamma}_{obs}\right|_i$ represents the observed InSAR coherence corresponding to the i-th interferometric pair, and $\left|\tilde{\gamma}(\alpha, h)\right|_i$ denotes the modeled coherence corresponding to the i-th interferometric pair.

To ensure that the estimated parameters meet practical accuracy requirements, a two-step nonlinear least-squares optimization strategy was adopted. First, an initial fitting was performed to obtain preliminary estimates of α and h based on Equation (7). In this stage, the model assumes that α and h are relatively independent to avoid convergence issues that may arise under highly nonlinear conditions. Subsequently, the estimated α and h obtained from the first fitting were used as the initial values for the second-stage nonlinear least squares optimization. In this stage, the interaction between α and h is jointly considered, and the complex interferometric coherence expression is reconstructed accordingly. The objective function for the second-stage nonlinear least squares optimization can be written as follows:

$$(\alpha', h') = \arg\min_{\alpha',h'} \sum_{i=1}^{n} \left\| \left| \tilde{\gamma}_{obs} \right|_i - \left| \tilde{\gamma}'(\alpha', h') \right|_i \right\|^2 \tag{8}$$

In forested areas, the phase information obtained from interferometric measurements essentially corresponds to the position of the dominant scattering phase center within the resolution cell, rather than the true ground surface. Therefore, to retrieve sub-canopy topography, the SPCH must first be derived from the complex coherence. This process can be expressed as

$$h_{SPCH} = \frac{arg\left(\tilde{\gamma}'\right)}{k_z} \tag{9}$$

where h_{SPCH} denotes the height of the SPCH. In the second-stage solution, the estimated forest parameters α' and h' are substituted into Equation (3) to compute the complex coherence $\tilde{\gamma}'$, and the interferometric phase is obtained from its argument $arg\left(\tilde{\gamma}'\right)$. Furthermore, Equation (9) establishes a quantitative relationship between the interferometric phase and the corresponding vertical elevation, enabling the conversion from phase to height. It should be noted that, in forested areas, the elevation derived from conventional InSAR measurements corresponds to the position of the scattering phase center, rather than the true ground surface. Therefore, it is necessary to estimate the SPCH through model inversion. This process retrieves forest structural parameters from observed coherence. It then reconstructs the coherence and the corresponding phase. Based on this, the conventional InSAR-derived DEM can be corrected using SPCH, allowing for a more accurate reconstruction of the true sub-canopy topography elevation.

4. Results and Accuracy Assessment of Sub-Canopy Topography Retrieval

In forested areas, large-scale DEM mapping using InSAR is significantly affected by vegetation volume scattering, which introduces considerable deviations between the InSAR-derived DEM and the actual terrain. To more clearly demonstrate the effectiveness of the proposed method in sub-canopy topography retrieval, a visual comparison was conducted within the LiDAR coverage area. Figure 2 shows the locations of the elevation profiles used for detailed comparison. The profiles are extracted along the black solid line in the figure. This path crosses representative terrain and vegetation types within the study area. These profiles allow a local assessment of the agreement between the retrieved sub-canopy topography and the reference data. The corresponding comparison results are presented in Figure 3.

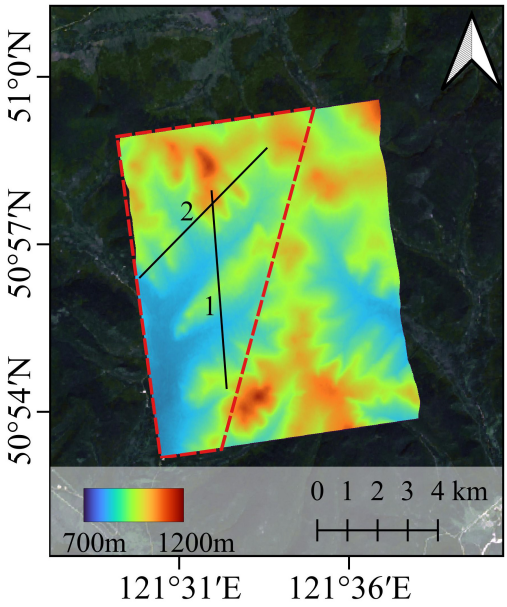


Figure 2. Location of the elevation profiles. The red dashed box indicates the LiDAR data coverage.

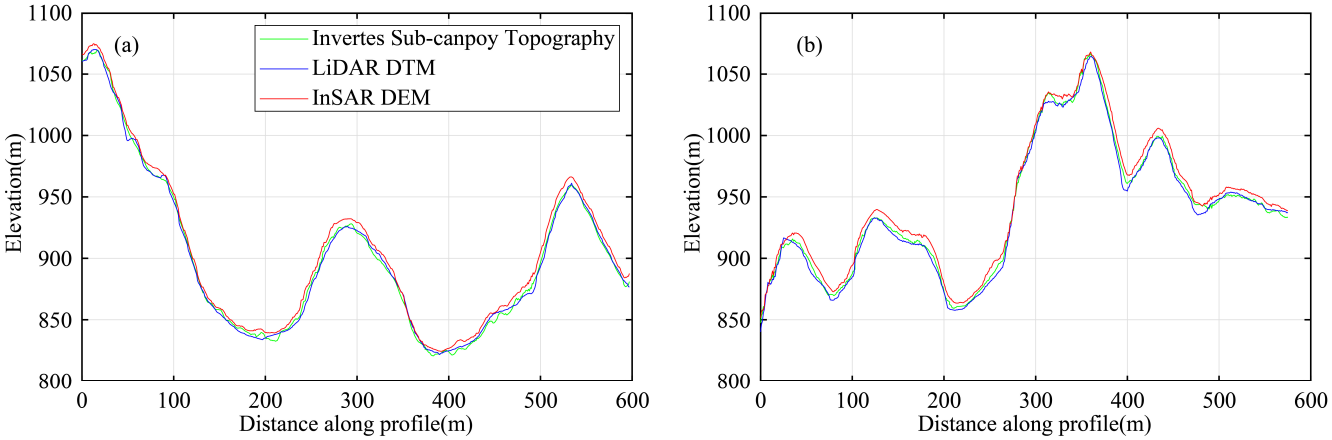


Figure 3. Elevation profiles: (**a**) Profile 1; (**b**) Profile 2.

Figure 3 shows the elevation residual distributions among the conventional InSAR-derived DEM, the sub-canopy topography retrieved using the proposed method, and the LiDAR-derived surface elevation. The elevation profile indicates that the conventional InSAR DEM is strongly affected by vegetation scattering, resulting in a scattering phase center height shift of approximately 0–10 m. Consequently, the elevations derived from

InSAR are generally higher than the ground elevations measured by LiDAR. After removing the influence of the scattering phase center, the sub-canopy topography retrieved by the proposed method agrees well with the LiDAR-derived surface elevation, providing a more accurate representation of the actual terrain. However, relatively large retrieval errors persist in some areas. This discrepancy is mainly attributed to the assumption that the pure ground-to-volume amplitude ratio μ_0 is treated as a globally fixed parameter in the retrieval model. In real forest environments, vegetation structure and canopy cover vary spatially, leading to changes in the relative contributions of ground scattering and volume scattering. As a result, deviations between the retrieved terrain and the actual terrain may still occur in certain local areas.

Pixel-wise accuracy assessment is conducted using LiDAR-derived surface elevation data, while point-wise validation is performed using ICESat-2 footprint data. The corresponding quantitative comparison results are shown in Figure 4a,c, illustrating the agreement among the InSAR-derived DEM, the retrieved sub-canopy topography, and the ICESat-2 and airborne LiDAR reference datasets. Compared with the ICESat-2 and LiDAR data, the InSAR-derived DEM exhibits relatively large errors, with root-mean-square errors (RMSE) of 6.65 m and 6.43 m, respectively. In contrast, the sub-canopy topography retrieved using the FVC-integrated IWCM shows significantly improved agreement with both reference datasets. Relative to the ICESat-2 data, the RMSE is reduced to 3.79 m, whereas in the LiDAR-based validation, it reaches 3.92 m. The coefficient of determination (R^2) further indicates a strong correlation (0.99) between the retrieved results and the reference data. These results demonstrate that introducing the FVC constraint effectively reduces the influence of forest volume scattering on the interferometric phase and improves the separation between ground scattering and volume scattering, thereby significantly enhancing the accuracy of sub-canopy topography retrieval. Overall, at a spatial resolution of 10 m, the FVC-integrated IWCM exhibits a more stable and reliable terrain reconstruction capability than the conventional InSAR-derived DEM, confirming the effectiveness of the proposed method in mitigating vegetation effects and recovering the true sub-canopy topography.

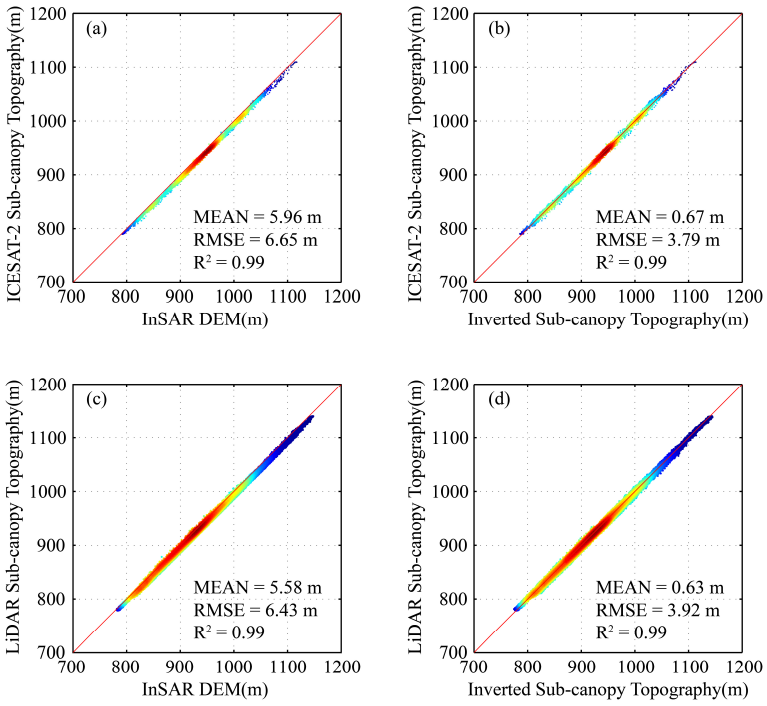


Figure 4. Accuracy validation of the InSAR DEM and the retrieved sub-canopy topography: (**a**,**c**) accuracy assessment of the InSAR DEM; (**b**,**d**) accuracy assessment of the sub-canopy topography retrieval results. (The colors from blue to red indicate increasing point density.).

5. Discussion

5.1. Influence of Forest Density on Retrieval Results

Forest density partly reflects the relative contributions of ground- and volume-scattering signals. Therefore, analyzing retrieval accuracy across different forest-density conditions is important for evaluating the proposed method's applicability. Previous studies have shown that FVC can be used to construct a forest density classification system, providing an effective basis for analyzing forest structural characteristics [33,34]. However, when forest density classes are defined using summer FVC data in the study area, the FVC values in some regions cannot be clearly associated with specific forest density levels. This is mainly due to factors such as differences in vegetation type, growth conditions, and seasonal variations, which limit a single FVC indicator's ability to fully represent forest canopy closure. Consequently, some uncertainty exists in the boundaries of forest density classification. To improve the stability and reliability of forest density classification, the range of FVC values used for classification was further refined based on the original FVC-based classification approach. In addition, the classification results were analyzed alongside the sub-canopy topography retrieval results to investigate how retrieval accuracy varies across different forest-density conditions.

Figure 5a,b adopt two different FVC interval classification strategies to analyze the response of sub-canopy topography retrieval errors (mean error and root-mean-square error) to variations in forest coverage. The retrieval results are validated using ICESat-2 and airborne LiDAR-derived surface elevation data as reference datasets. Since FVC effectively characterizes forest density and canopy structural variability, and forest density directly influences the relative contributions of volume scattering and ground scattering, the retrieval accuracy exhibits noticeable variations with changes in FVC.

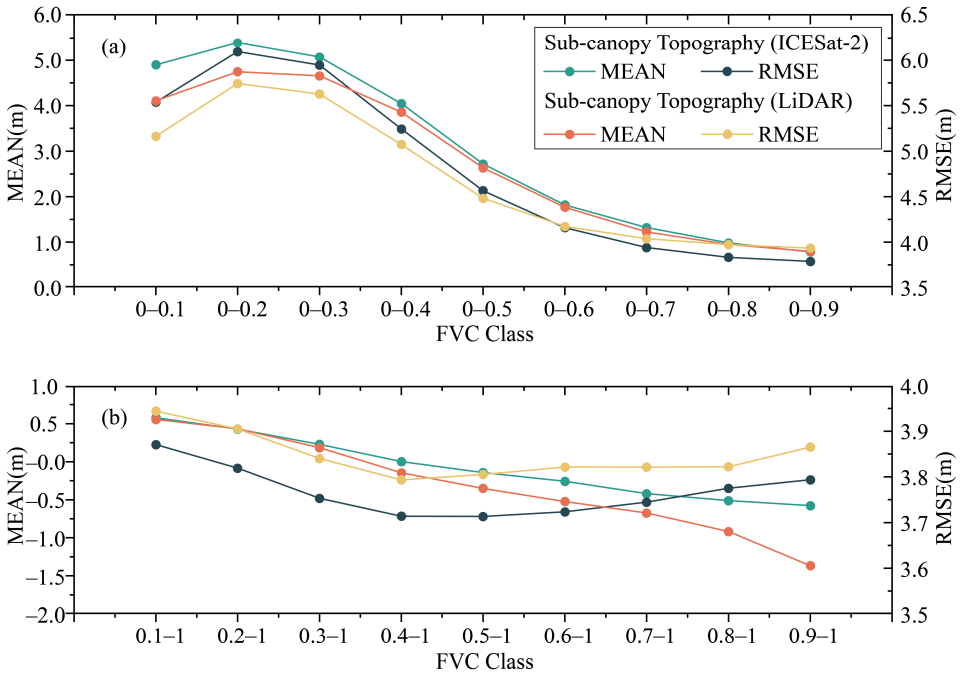


Figure 5. Accuracy validation of sub-canopy topography under different FVC intervals: (**a**) upper-limit increasing interval (0–x); (**b**) lower-limit increasing interval (x–1).

In Figure 5a, the FVC interval expands progressively from 0–0.1 to 0–0.9, reflecting the trend of error variation as forest density increases. The validation results from ICESat-2 and LiDAR are generally consistent. In low-density regions (0–0.1 and 0–0.2), the errors reach their peak values, with RMSEs of 6.10 m and 5.74 m, respectively. This is mainly

because ground scattering dominates and land cover types are relatively complex, making it difficult to effectively separate volume scattering from ground scattering. As FVC increases (from 0–0.3 to 0–0.6), canopy continuity improves and the contribution of volume scattering increases, resulting in a significant reduction in both MEAN and RMSE. In higher coverage ranges (0–0.7 to 0–0.9), the errors further decrease and stabilize, with RMSE values of approximately 3.9 m and mean error (MEAN) values approaching zero, indicating good model stability under these conditions.

In contrast, Figure 5b adopts interval classifications ranging from 0.1–1 to 0.9–1, progressively concentrating samples in high-density forest areas. When the lower bound of the interval is relatively low (0.1–1 and 0.2–1), the inclusion of low-density pixels results in relatively large and fluctuating errors. As the FVC lower bound increases (from 0.3–1 to 0.7–1), the retrieval accuracy improves significantly, with RMSE decreasing to approximately 3.43 m and MEAN approaching zero, indicating improved model stability under moderate-to-high forest density conditions. However, in extremely high coverage intervals (0.8–1 and 0.9–1), the errors show a slight increase. This is mainly attributed to the reduced penetration capability of radar signals under dense canopy conditions and the enhanced volume scattering, which exerts a stronger influence on the scattering phase center.

Overall, forest density significantly affects the accuracy of sub-canopy topography retrieval by regulating the relative contributions of volume scattering and ground scattering. The proposed method performs best under moderate to relatively high forest density conditions, where the model assumptions are better satisfied, and the retrieval results are more stable and reliable.

5.2. Influence of Slope on Retrieval Results

The accuracy assessment results presented in Section 4 indicate that some validation points exhibit relatively large retrieval errors, which are mainly concentrated in areas with pronounced terrain variation [35]. As shown in Figure 1c, the forest region of Genhe City is characterized by complex terrain and significant slope variation. Therefore, topographic factors, particularly slope, may have an important influence on the sub-canopy topography retrieval results. To further investigate the causes of these errors, slope was selected as the primary variable for analysis in this section. The validation points were first grouped into different slope intervals, and statistical analyses were then conducted for each slope class. By comparing the retrieval results under different slope conditions, the influence of slope variation on the accuracy of sub-canopy topography retrieval can be systematically evaluated.

Figure 6 illustrates the accuracy of sub-canopy topography retrieval evaluated using ICESat-2 and airborne LiDAR data under different slope intervals. Overall, the RMSE values derived from both reference datasets increase with slope. In steeper slope intervals (e.g., 15–20°, 20–25°, and 25–30°), the RMSE remains at approximately 4–5 m, indicating a clear degradation in retrieval accuracy under steep terrain conditions. In contrast, in areas with gentle slopes, the RMSE gradually decreases, suggesting that flatter terrain is more favorable for terrain reconstruction.

In terms of MEAN, both ICESat-2 and LiDAR exhibit a positive bias in high-slope intervals, indicating that the retrieved elevations are generally slightly higher than the reference terrain. Conversely, in low-slope intervals (e.g., 0–3° and 0–5°), both datasets show slight negative biases, suggesting a tendency toward underestimation in relatively flat areas. These error characteristics are primarily related to the influence of complex terrain conditions on the remote sensing observation process. In steep areas, the angle between the radar line of sight and the terrain surface varies significantly, which can lead to geometric distortions such as foreshortening and layover, as well as shifts in the scattering phase center. These effects make it difficult to effectively separate volume scattering from ground

scattering. Meanwhile, the complex imaging geometry and signal propagation conditions increase the uncertainty of model parameters, weakening the ability of the dual-baseline IWCM to constrain the coupling between attenuation coefficient and forest height, thereby reducing retrieval stability and accuracy.

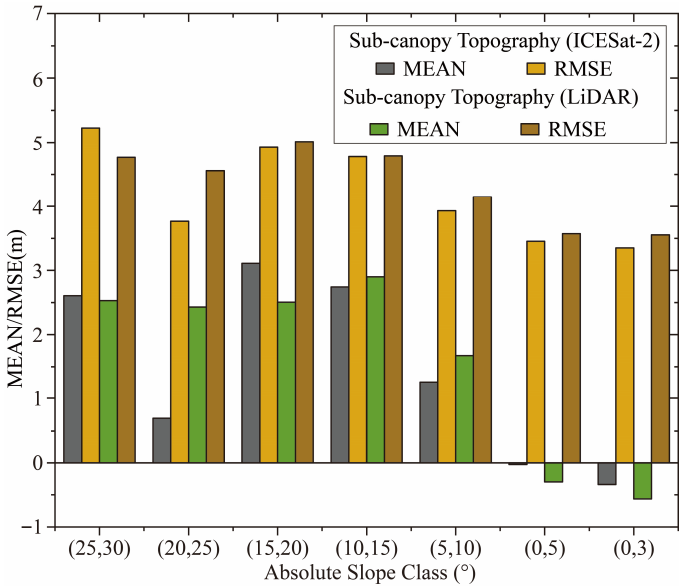


Figure 6. Accuracy validation of sub-canopy topography under different slope intervals.

In addition, terrain variability may also affect the accuracy of ICESat-2 measurements. Factors such as slope inclination and waveform mixing can introduce local elevation biases that may further amplify overall retrieval errors.

Overall, slope is a critical factor affecting the accuracy of sub-canopy topography retrieval. As the slope increases, the complexity of imaging geometry and signal propagation introduces greater uncertainty, leading to reduced retrieval accuracy. Future work could improve performance in complex terrain by incorporating slope correction strategies, multi-view geometric constraints, or slope-aspect analysis.

5.3. Influence of μ_0 on Retrieval Results

Within the modeling framework developed in this study, the parameter configuration has been modified compared with previous work. This change directly affects the optimal range and stability of μ_0. Therefore, it is necessary to redefine μ_0 and analyze its sensitivity and the propagation of uncertainty in the retrieval results.

Following the approach adopted in previous studies, the backscattering amplitudes of bare soil and dense vegetation areas were re-estimated and statistically characterized. A multi-sample dataset was then constructed to represent the potential range of μ_0. Based on this dataset, ten representative values of μ_0 (0.05, 0.15, 0.25, 0.35, 0.45, 0.55, 0.65, 0.75, 0.85, and 0.95) were selected within the study area. Under the condition that all other model parameters were kept constant, a series of sub-canopy topography retrieval experiments was conducted. By comparing the retrieval results corresponding to different μ_0 values, the response characteristics of the model to variations in μ_0 were systematically evaluated.

As shown in Figure 7a, the accuracy of sub-canopy topography retrieval under different μ_0 values exhibits a consistent trend across the full slope range. With increasing μ_0, the error metrics derived from both ICESat-2 and LiDAR-derived surface elevation show an approximately monotonic increase, indicating that overly large μ_0 values introduce both systematic and random errors. The errors derived from LiDAR are generally higher than

those from ICESat-2, suggesting that high-precision reference data are more sensitive to parameter perturbations. Under these conditions, the optimal value of μ_0 is 0.35.

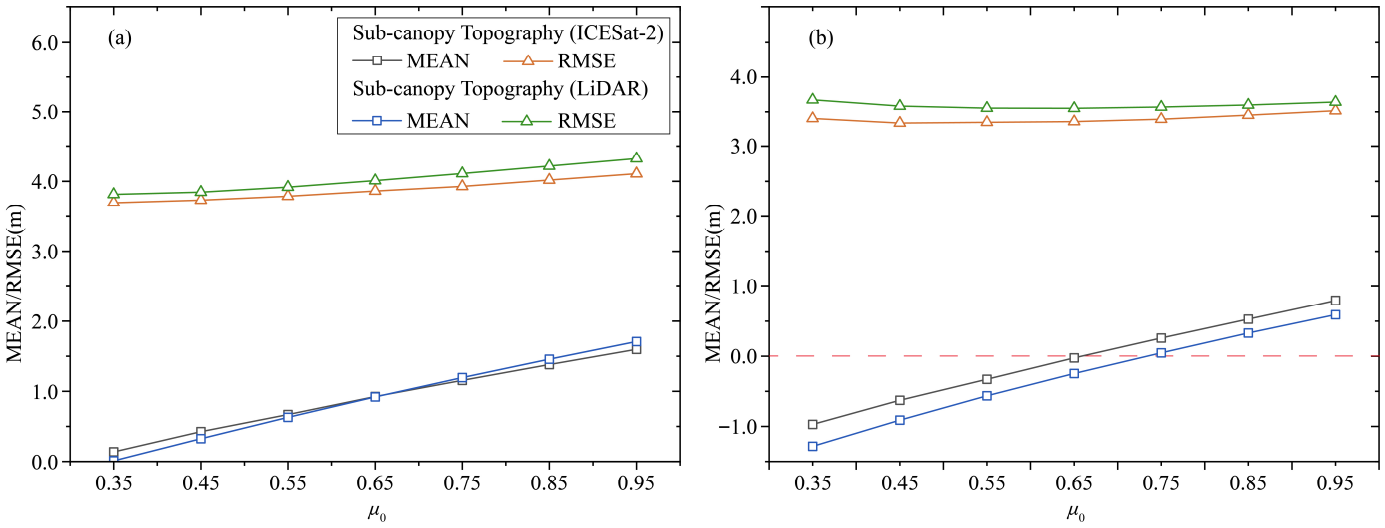


Figure 7. Influence of different μ_0 values on sub-canopy topography retrieval accuracy: (**a**) full slope range; (**b**) low-slope range $[-3°, 3°]$.

The influence of μ_0 was further analyzed within flat terrain conditions (slope range of $[-3°, 3°]$) as shown in Figure 7b. It can be observed that the overall error level is significantly reduced. The MEAN gradually shifts from a negative bias to a positive bias as μ_0 increases, approaching zero at $\mu_0 = 0.65$, indicating that this value effectively mitigates systematic error. In contrast, the RMSE exhibits only minor fluctuations, suggesting that under gentle terrain conditions, the model remains relatively stable and is less sensitive to variations in μ_0.

A comparison between the results over the full slope range and those under low-slope conditions reveals a clear coupling relationship between μ_0 and terrain slope. Across the full slope range, slope-induced geometric distortions and variations in scattering mechanisms reduce interferometric coherence and amplify errors caused by deviations in μ_0, leading to instability in its optimal value. In contrast, in flat areas, the influence of terrain is reduced, and μ_0 primarily reflects the difference between bare-soil scattering and vegetation scattering. Its role becomes more stable and is mainly manifested in the adjustment of systematic bias.

Overall, terrain slope influences both the effective range and sensitivity of μ_0 by affecting interferometric signal quality and scattering characteristics. Therefore, in practical applications, μ_0 should be determined using terrain-dependent or adaptive strategies to improve the accuracy and stability of sub-canopy topography retrieval in complex terrain conditions.

5.4. Comparative Analysis of Retrieval Results Using FVC and NDVI Vegetation Parameters

In forested areas, the total backscattering observed by InSAR consists of three components: ground backscattering, ground backscattering attenuated by the canopy, and volume scattering attenuated by the canopy. Compared with bare land or areas with sparse vegetation, the presence of numerous vegetation scatterers within the forest canopy significantly enhances the volume-scattering component. As a result, the elevation measured by InSAR corresponds to the scattering phase center located between the canopy and the ground surface. As vegetation coverage increases, the proportion of volume scattering becomes larger, and the scattering phase center height shifts upward accordingly. Vegetation indices are fundamental data for characterizing surface vegetation conditions, among which the NDVI and FVC are the most widely used [34,36].

In InSAR-based sub-canopy topography retrieval models, the volume scattering term is often estimated using empirical parameters when effective constraints on vegetation coverage are lacking. Introducing FVC as a constraint variable can improve the physical consistency of volume scattering modeling. Building on previous studies using NDVI [17], this study focuses on the physical role of FVC in constraining model parameters. It examines how its uncertainty affects the retrieval results for sub-canopy topography.

NDVI is calculated from the reflectance of the near-infrared and red bands. It primarily represents vegetation spectral response and physiological activity and is widely used for regional-scale vegetation monitoring. However, under the dense vegetation conditions of the study area (Figure 8a), NDVI shows a relatively smooth spatial distribution and low contrast in dense forest regions (Figure 8b). This indicates a clear saturation effect, which limits its ability to capture spatial variations in vegetation structure. In contrast, FVC represents the proportion of ground covered by vegetation. It focuses on the horizontal spatial distribution of vegetation (Figure 8c). Its spatial pattern is more discrete and heterogeneous, allowing clearer differentiation of canopy density across regions. Since InSAR volume scattering depends primarily on the number of vegetation scatterers rather than on spectral response alone, FVC can more directly reflect scattering contributions. It is therefore more physically consistent with the volume scattering weighting parameter. As a result, compared with NDVI, FVC provides a more effective constraint for modeling ground and volume scattering and leads to improved accuracy in sub-canopy topography retrieval.

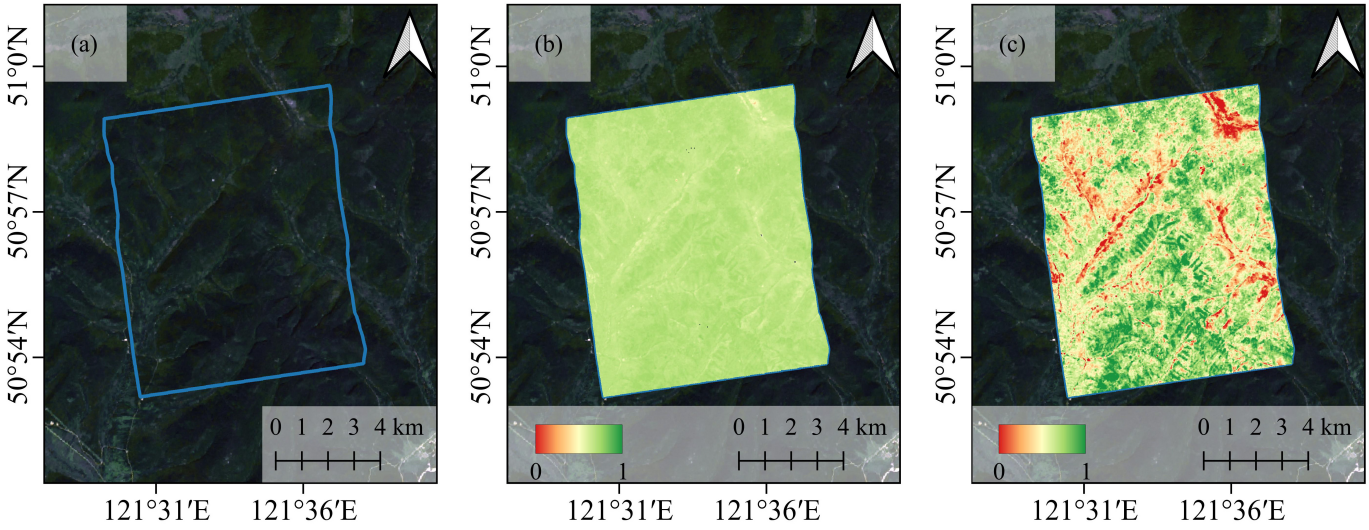


Figure 8. Vegetation distribution in the study area: (**a**) optical remote sensing image of the study area (blue solid box indicates the extent of the study area); (**b**) NDVI; (**c**) FVC.

Based on the determination of the optimal μ_0 under different vegetation parameter conditions, a comparative analysis was conducted between the retrieval results from the FVC-based method and those from the previously proposed NDVI-based method. It should be noted that μ_0 is not an independent parameter; its optimal value depends on the representation of vegetation parameters. Therefore, to ensure a fair comparison, the respective optimal μ_0 values for each method were adopted.

As shown in Table 2, the two vegetation parameters exhibit distinct retrieval performance under their optimal μ_0 conditions. The optimal μ_0 is 0.55 for NDVI and 0.65 for FVC, indicating a clear coupling relationship between μ_0 and vegetation parameters. Under these conditions, the FVC-based approach achieves higher accuracy for both reference datasets. In particular, for the LiDAR-derived surface elevation, the RMSE decreases from

4.02 m to 3.55 m, corresponding to an improvement of 11.69%, which suggests that FVC more effectively characterizes vegetation scattering properties.

Table 2. Comparison of retrieval accuracy for different vegetation parameters under optimal μ_0 conditions.

Vegetation Parameter	Baseline Number	Slope (°)	Optimal μ_0	ICESat-2		LiDAR	
				MEAN (m)	RMSE (m)	MEAN (m)	RMSE (m)
NDVI	3	$[-3°, 3°]$	0.55	−0.71	3.37	0.23	4.02
FVC	2		0.65	−0.02	3.36	−0.25	3.55

6. Conclusions

This study proposes a TanDEM-X dual-baseline InSAR method for retrieving sub-canopy topography. The method integrates FVC with a two-step nonlinear least squares optimization strategy. It is validated using ICESat-2 and airborne LiDAR data. The results show that combining optical and radar information significantly improves retrieval accuracy and enhances parameter estimation stability. Compared with the original InSAR-derived DEM, the RMSE decreases from 6.43 m to 3.92 m, corresponding to an improvement of about 39.04%. Compared with the NDVI-based method, the RMSE decreases from 4.02 m to 3.55 m, with an additional improvement of about 11.69%.

From a physical perspective, FVC constrains the relative contributions of ground and volume scattering. It does this by establishing a nonlinear relationship with the ground-to-volume amplitude ratio. This improves the model's physical consistency. Under moderate forest density conditions, ground and volume scattering are balanced. Under these conditions, the retrieval accuracy reaches its optimal level.

In terms of performance, the FVC-based model shows lower systematic bias and higher overall accuracy than the NDVI-based method. Compared with the conventional InSAR DEM and the NDVI-based approach, the proposed method better suppresses vegetation effects and improves physical consistency. These results confirm its effectiveness in characterizing vegetation scattering in complex forest environments.

However, some limitations remain. The model assumes a constant μ_0 across the study area. This may not fully represent the spatial heterogeneity of forest structure. In addition, the retrieval results are sensitive to terrain conditions, especially slope. Terrain affects imaging geometry and signal propagation. In high-density forest areas, reduced radar signal penetration may also limit the method's performance. This may restrict its applicability in complex environments.

Future work should focus on several aspects. Adaptive or spatially varying estimation of μ_0 should be developed to better capture spatial heterogeneity. Multi-baseline InSAR observations can be used to improve the robustness of the inversion. Terrain correction strategies should be introduced to reduce topographic effects. The method should also be validated across different forest types and environmental conditions to improve its generalization capability.

From a broader application perspective, accurate sub-canopy topography has important ecological and societal value. It supports forest resource management, carbon cycle assessment, and ecological monitoring, especially in boreal forest regions that play a key role in the global climate system. It can also provide essential data for natural hazard analysis, such as flood simulation and landslide risk assessment. These applications highlight the practical value of the proposed method.

Author Contributions: Conceptualization, Z.F. and H.W.; methodology, Z.F. and H.W.; software, Z.F. and H.W.; validation, Z.F. and H.W.; formal analysis, Z.F. and H.W.; investigation, Z.F. and H.W.; resources, H.W. and R.L.; data curation, Z.F. and H.W.; writing—original draft preparation, Z.F. and H.W.; writing—review and editing, Z.F., H.W., X.M. (Xiangwei Meng), L.Z. and X.M. (Xiaoming Ma); visualization, Z.F. and H.W.; supervision, Z.F., H.W., X.M. (Xiangwei Meng), L.Z. and X.M. (Xiaoming Ma); project administration, H.W. and R.L.; funding acquisition, H.W. and R.L. All authors have read and agreed to the published version of the manuscript.

Funding: This research was funded by the High-level/excellent doctoral talents introduction research project in Inner Mongolia Agricultural University (NDYB2022-27); the National Natural Science Foundation of China (52269004); the State Key Laboratory of Water Engineering Ecology and Environment in Arid Areas, Inner Mongolia Agricultural University (SQ2024SKL08048); the National Natural Science Foundation of China (No. 42204024); and the Natural Science Foundation project of Inner Mongolia (2024MS04006).

Data Availability Statement: The ICESat-2 data used in this article can be downloaded for free or ordered through the following link: https://nsidc.org/data/data-access-tool/ATL08/versions/6 (accessed on 5 March 2024). The TanDEM-X data can be obtained from the German Aerospace Center (DLR).

Acknowledgments: The authors would also like to acknowledge the German Aerospace Center (DLR) for providing the TanDEM-X data over study areas (ID. NTI_BIST7299) and the National Snow and Ice Data Center for providing the ICESAT-2 data.

Conflicts of Interest: The authors declare no conflicts of interest.

References

1. Zhang, S.; Wang, J.; Feng, Z.; Wang, J.; Li, J.; Liu, N. Verification of the accuracy of Sentinel-1 for DEM extraction error analysis under complex terrain conditions. *Int. J. Appl. Earth Obs. Geoinf.* **2024**, *133*, 104157. [CrossRef]
2. Rijal, S.; Wang, G.; Woodford, P.B.; Howard, H.R.; Hutchinson, J.M.S.; Hutchinson, S.; Schoof, J.; Oyana, T.J.; Li, R.; Park, L.O. Detection of gullies in Fort Riley military installation using LiDAR derived high resolution DEM. *J. Terramech.* **2018**, *77*, 15–22. [CrossRef]
3. Wang, N.; Cheng, W.; Wang, B.; Liu, Q.; Zhou, C. Geomorphological regionalization theory system and division methodology of China. *J. Geogr. Sci.* **2020**, *30*, 212–232. [CrossRef]
4. Liu, X.; Xu, G.; Yi, Y.; Zhang, T.; Xia, Y. A Novel Approach to Generate Large-Scale InSAR-Derived Velocity Fields: Enhanced Mosaicking of Overlapping InSAR Data. *Remote Sens.* **2025**, *17*, 1804. [CrossRef]
5. Chen, Y.; Shi, Z.; Eziz, A.; Zheng, S.; Ilniyaz, O.; Azadi, H.; Van de Voorde, T.; Kurbana, A. Improving altitudinal accuracy of Sentinel-1 InSAR DEM in arid flat terrain: A machine learning approach with UAV photogrammetry and multi-source data. *Geo-Spat. Inf. Sci.* **2025**, 1–23. [CrossRef]
6. González, C.; Bräutigam, B. Relative height accuracy estimation method for InSAR-based DEMs. *IEEE J. Sel. Top. Appl. Earth Obs. Remote Sens.* **2015**, *8*, 5352–5360. [CrossRef]
7. Dong, J.; Jiang, H.; Xu, M.; Gao, K. A novel InSAR-based workflow for DEM-driven slope modeling and risk prediction. *Geomat. Nat. Hazards Risk* **2025**, *16*, 2598439. [CrossRef]
8. Xie, Y.; Zhu, J.; Fu, H.; Wang, C. A review of underlying topography estimation over forest areas by InSAR: Theory, advances, challenges and perspectives. *J. Cent. South Univ.* **2020**, *27*, 997–1011. [CrossRef]
9. Zhang, T.; Fu, H.; Zhu, J.; Lopez-Sanchez, J.M.; Gómez, C.; Wang, C. Estimation of canopy height from a multi-SINC model in mediterranean forest with single-baseline TanDEM-X InSAR data. *IEEE J. Sel. Top. Appl. Earth Obs. Remote Sens.* **2024**, *17*, 5484–5499. [CrossRef]
10. Chen, H.; Cloude, S.R.; Goodenough, D.G. Forest canopy height estimation using Tandem-X coherence data. *IEEE J. Sel. Top. Appl. Earth Obs. Remote Sens.* **2016**, *9*, 3177–3188. [CrossRef]
11. Olesk, A.; Praks, J.; Antropov, O.; Zalite, K.; Arumäe, T.; Voormansik, K. Interferometric SAR coherence models for characterization of hemiboreal forests using TanDEM-X data. *Remote Sens.* **2016**, *8*, 700. [CrossRef]
12. Liu, Z.; Zhu, J.; Lopez-Sanchez, J.M.; Gómez, C.; Fu, H.; Zhou, C. Simultaneous estimation of subcanopy topography and forest height with single-baseline single-polarization TanDEM-X interferometric data combined with ICESat-2 data. *IEEE J. Sel. Top. Appl. Earth Obs. Remote Sens.* **2024**, *17*, 11598–11617. [CrossRef]
13. Gómez, C.; Lopez-Sanchez, J.M.; Romero-Puig, N.; Zhu, J.; Fu, H.; He, W. Canopy height estimation in Mediterranean forests of Spain with TanDEM-X data. *IEEE J. Sel. Top. Appl. Earth Obs. Remote Sens.* **2021**, *14*, 2956–2970. [CrossRef]

14. Olesk, A.; Voormansik, K.; Vain, A.; Noorma, M.; Parks, J. Seasonal differences in forest height estimation from interferometric TanDEM-X coherence data. *IEEE J. Sel. Top. Appl. Earth Obs. Remote Sens.* **2015**, *8*, 5565–5572. [CrossRef]
15. Zhao, L.; Chen, E.; Li, Z.; Zhang, W.; Fan, Y. A new approach for forest height inversion using X-band single-pass InSAR coherence data. *IEEE Trans. Geosci. Remote Sens.* **2021**, *60*, 5206018. [CrossRef]
16. Wang, H.; Feng, Z.; Li, R.; Yu, Y. Sub-Canopy Topography Inversion Using Multi-Baseline Bistatic InSAR Without External Vegetation-Related Data. *Remote Sens.* **2026**, *18*, 231. [CrossRef]
17. Wang, H.; Feng, Z.; Fu, H.; Zhu, J.; Li, R.; Liu, Z.; Wang, L.; Hao, S.; Zhang, Q.; Zhao, L.; et al. High-resolution subcanopy topography inversion for boreal forest areas based on an IWCM-aided multi-baseline InSAR method. *ISPRS-J. Photogramm. Remote Sens.* **2025**, *230*, 547–562. [CrossRef]
18. Zhao, W.; Zhang, B.; Hu, Z.; Zhang, J.; Song, W. Adaptive Neighborhood Aggregation Algorithm for PolInSAR Forest Height Estimation. *Sci. Remote Sens.* **2026**, *13*, 100385. [CrossRef]
19. Cloude, S.R.; Papathanassiou, K.P. Polarimetric SAR interferometry. *IEEE Trans. Geosci. Remote Sens.* **1998**, *36*, 1551–1565. [CrossRef]
20. Luo, H.; Yue, C.; Wu, Y.; Zhang, X.; Lu, C.; Ou, G. An efficient method for estimating tropical forest canopy height from airborne PolInSAR data. *Ecol. Indic.* **2024**, *166*, 112566. [CrossRef]
21. Zhang, B.; Li, J.; Zhang, J.; Ren, D.; Song, W.; Zhu, J.; Zhou, C. PolSAR Forest Height Inversion Based on Multi-Class Feature Fusion. *Remote Sens.* **2026**, *18*, 946. [CrossRef]
22. Vepakomma, U.; Kneeshaw, D.; Fortin, M.J. Spatial contiguity and continuity of canopy gaps in mixed wood boreal forests: Persistence, expansion, shrinkage and displacement. *J. Ecol.* **2012**, *100*, 1257–1268. [CrossRef]
23. Askne, J.I.H.; Ulander, L.M.H. Boreal forest properties from TanDEM-X data using interferometric water cloud model and implications for a bistatic C-band mission. *IEEE J. Sel. Top. Appl. Earth Obs. Remote Sens.* **2021**, *14*, 8627–8637. [CrossRef]
24. Santoro, M.; Wegmüller, U.; Askne, J. Forest stem volume estimation using C-band interferometric SAR coherence data of the ERS-1 mission 3-days repeat-interval phase. *Remote Sens. Environ.* **2018**, *216*, 684–696. [CrossRef]
25. Askne, J.; Santoro, M. Multitemporal repeat pass SAR interferometry of boreal forests. *IEEE Trans. Geosci. Remote Sens.* **2005**, *43*, 1219–1228. [CrossRef]
26. Krieger, G.; Moreira, A.; Fiedler, H.; Hajnsek, I.; Werne, M.; Younis, M. TanDEM-X: A satellite formation for high-resolution SAR interferometry. *IEEE Trans. Geosci. Remote Sens.* **2007**, *45*, 3317–3341. [CrossRef]
27. Zink, M.; Bachmann, M.; Brautigam, B.; Fritz, T.; Hajnsek, I.; Moreira, A. TanDEM-X: The new global DEM takes shape. *IEEE Trans. Geosci. Remote Sens.* **2014**, *2*, 8–23. [CrossRef]
28. Rizzoli, P.; Martone, M.; Gonzalez, C.; Wecklich, C.; Borla Tridon, D.; Bräutigam, B.; Bachmann, M.; Schulze, D.; Fritz, T.; Huber, M.; et al. Generation and performance assessment of the global TanDEM-X digital elevation model. *ISPRS-J. Photogramm. Remote Sens.* **2017**, *132*, 119–139. [CrossRef]
29. Loveland, T.R.; Irons, J.R. Landsat 8: The plans, the reality, and the legacy. *Remote Sens. Environ.* **2016**, *185*, 1–6. [CrossRef]
30. Markus, T.; Neumann, T.; Martino, A.; Abdalati, W.; Brunt, K.; Csatho, B.; Farrell, S.; Fricker, H.; Gardner, A.; Harding, D.; et al. The Ice, Cloud, and land Elevation Satellite-2 (ICESat-2): Science requirements, concept, and implementation. *Remote Sens. Environ.* **2017**, *190*, 260–273. [CrossRef]
31. Soja, M.J.; Askne, J.I.H.; Ulander, L.M.H. Estimation of boreal forest properties from TanDEM-X data using inversion of the interferometric water cloud model. *IEEE Geosci. Remote Sens. Lett.* **2017**, *14*, 997–1001. [CrossRef]
32. Wang, H.; Fu, H.; Zhu, J.; Liu, Z.; Zhang, B.; Wang, C.; Li, Z.; Hu, J.; Yu, Y. Estimation of subcanopy topography based on single-baseline TanDEM-X InSAR data. *J. Geod.* **2021**, *95*, 84. [CrossRef]
33. Song, W.; Mu, X.; Ruan, G.; Gao, Z.; Li, L.; Yan, G. Estimating fractional vegetation cover and the vegetation index of bare soil and highly dense vegetation with a physically based method. *Int. J. Appl. Earth Obs. Geoinf.* **2017**, *58*, 168–176. [CrossRef]
34. Zhang, Z.; Dong, X.; Tian, J.; Tian, Q.; Xi, Y.; He, D. Stand density estimation based on fractional vegetation coverage from Sentinel-2 satellite imagery. *Int. J. Appl. Earth Obs. Geoinf.* **2022**, *108*, 102760. [CrossRef]
35. Guo, R.; Li, S.; Chen, Y.; Li, X.; Yuan, L. Identification and monitoring landslides in Longitudinal Range-Gorge Region with InSAR fusion integrated visibility analysis. *Landslides* **2021**, *18*, 551–568. [CrossRef]
36. De La Iglesia Martinez, A.; Labib, S.M. Demystifying normalized difference vegetation index (NDVI) for greenness exposure assessments and policy interventions in urban greening. *Environ. Res.* **2023**, *220*, 115155. [CrossRef] [PubMed]

Disclaimer/Publisher's Note: The statements, opinions and data contained in all publications are solely those of the individual author(s) and contributor(s) and not of MDPI and/or the editor(s). MDPI and/or the editor(s) disclaim responsibility for any injury to people or property resulting from any ideas, methods, instructions or products referred to in the content.